Study of Electromagnetic Resonance Conditions in Interior Permanent Magnet Synchronous Motor (IPMSM)

Hiroki Sakamoto,
Norihisa Anegawa,
Shohei Suzuta

Keywords Sound vibration, Resonance condition, IPMSM

Abstract

Since the Interior Permanent Magnet Synchronous Motor (IPMSM) features a high power density and high efficiency, it is widely applied to industrial equipment and the Electric Vehicles (EVs). EVs require low noise performance. The IPMSM, a main component of the EV, is therefore required to improve its sound vibration characteristics. The major cause of its sound and vibration is the electromagnetic force generated between the stator core and the rotor and the resultant resonance.

In order to clarify the resonance conditions, we tried to single out an analytical model of the stator core to investigate characteristics of the electromagnetic force definitely. As a result, we found a resonance condition that had not be formerly reported. If the result of our study is adequately applied, it is possible to realize a resonance averting design for the stator core in order to contribute to the improvement of sound vibration characteristics for the IPMSM.

1 Preface

Since the Interior Permanent Magnet Synchronous Motor (IPMSM) features a high power density and high efficiency, it is widely used in industrial equipment. In recent years, compact motor design and higher speed are attempted for the purpose of product mass reduction. Due to the effect of such industrial trends, magnetic flux density in the motor interior tends to increase and radial electromagnetic excitation force is intensified. These difficulties are causing various sound and vibration issues.

The radial excitation force causes a ring mode in the stator core and motor case and this is a major factor of metallic radiation noise generated from the motor case. Research into such radiation noise has been frequently carried out and many reports have been released. In regard to resonance conditions, however, they are not fully clarified yet. In this paper, the electromagnetic force of the IPMSM is firstly defined as a harmonic excitation by making Fourier transformation in regard to space and time. This paper also introduces our study where a model of a finite element method reduced into a 48-degree-of-freedom is used to clarify the resonance conditions of the stator core and electromagnetic force.

2 Electromagnetic Force Characteristics of the IPMSM

2.1 Method of Electromagnetic Field Analysis

In the IPMSM, there is a slight space (air gap) between the stator core and the rotor. Magnetic flux is naturally concentrated in this air gap and harmonic magnetic flux of the stator core and the rotor causes mutual interference. The electromagnetic force generated as a result of this mutual interference causes excitation of the stator core. It is well known a fact that this phenomenon is one of causes of noise generation. For this reason, it is necessary to analyze resonance conditions relating to electromagnetic force and stator core in order to achieve noise reduction.

Fig. 1 shows a cross-sectional view of an 8-pole 48-slot IPMSM. The object of analysis is an 8-pole 48-slot IPMSM generally adopted for Electric Vehicles (EVs). With this model, two-dimensional electromagnetic field analysis was carried out with general-purpose analytical software. In consider-

ation of aperiodicity, a $\pi/4$ model was used for the analytical model and calculation was performed on the assumption that one period of electrical angle ($\pi/2$) corresponds to 181 steps. Given the rotational speed of the rotor is f_r, the current frequency f_e is $4f_r$ because the number of pairs of poles is 4. For the source current period T_e, $T_e = 1/f_e = 1/(4f_r)$. The measuring position of magnetic flux density is assumed to stay in the center of the air gap and the radial and peripheral magnetic flux density B_r and B_θ were derived at each time step. It is generally known that the electromagnetic force exerted on the respective teeth is comparatively strong[(1)]. For this reason, the radial electromagnetic force had been examined. Using the magnetic flux density already known, the radial electromagnetic force (Lorentz force) σ_r exerted on the air gap was derived from Expression (1) below.

$$\sigma_r = \frac{1}{2\mu_0}(B_r^2 - B_\theta^2) \cdots\cdots (1)$$

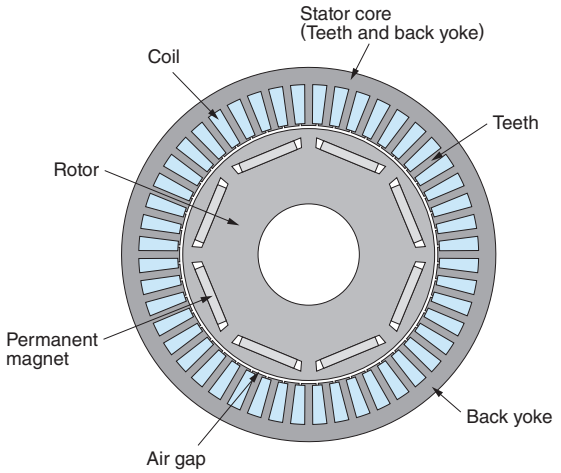

Fig. 1 Cross-Sectional View of 8-Pole 48-Slot IPMSM

As an objective model for analysis, the cross-sectional shape and part names of an 8-pole 48-slot IPMSM are shown.

Where, μ_0 is magnetic permeability under vacuum. The obtained electromagnetic force was processed by Fourier transformation※1, and the amplitude and phase at each order were then calculated to clarify the electromagnetic force distribution that was exerted on the stator core.

2.2 Result of Electromagnetic Field Analysis

Fig. 2 shows changes in flux lines with time. In order to examine the overall distribution of flux lines, the model shown in Fig. 2 is expressed as a π model where the analytical result is extended. Using Expression (1), the magnetic flux density obtained by electromagnetic field analysis is converted into a radial electromagnetic force. Fig. 3 shows changes in radial electromagnetic force with time. Angles shown in this figure denote rotor's rotational angles. According to Figs. 2 and 3, it is evident that the radial electromagnetic force is revolving with the rotor motion.

Fig. 4 shows a spatial distribution of electromagnetic force in a radial direction. The axis of abscissas shows the peripheral angle and that of ordinates shows Value σ_r. Fig. 5 shows the result of Fourier transformation on space. The axis of abscissas shows the nodal diameter κ that expresses the shape of special distribution and that of ordinates shows the amplitude. Pictures in this figure show shapes of special distribution at nodal diameter κ. It was recognized that the nodal diameter κ contains the integer multiples of 8.

Fig. 6 shows the change in amplitude with time for nodal diameter number 8. This figure indicates that the amplitude at nodal diameter number $\kappa = 8$ changes with time. Fig. 7 shows the relationship between electrical angle order and amplitude. According to the result of Fourier transformation on electromagnetic force at a single period of electrical

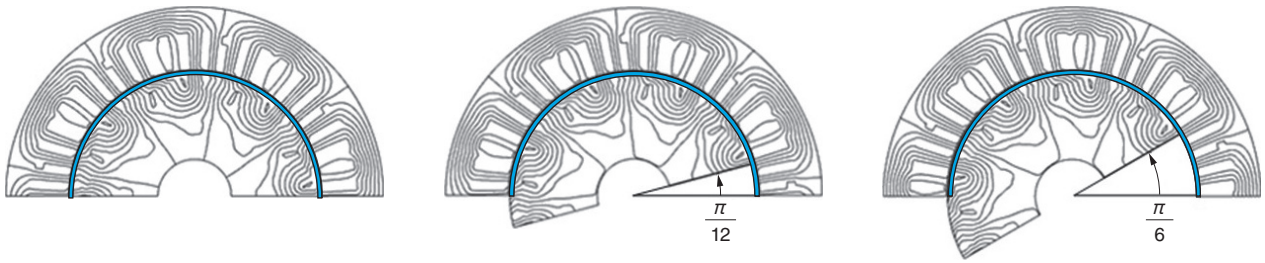

(a) t/Te = 0 (b) t/Te = 1/6 (c) t/Te = 1/3

Fig. 2 Changes in Flux Lines with Time

The diagrams show that flux lines are rotated together with the rotor.

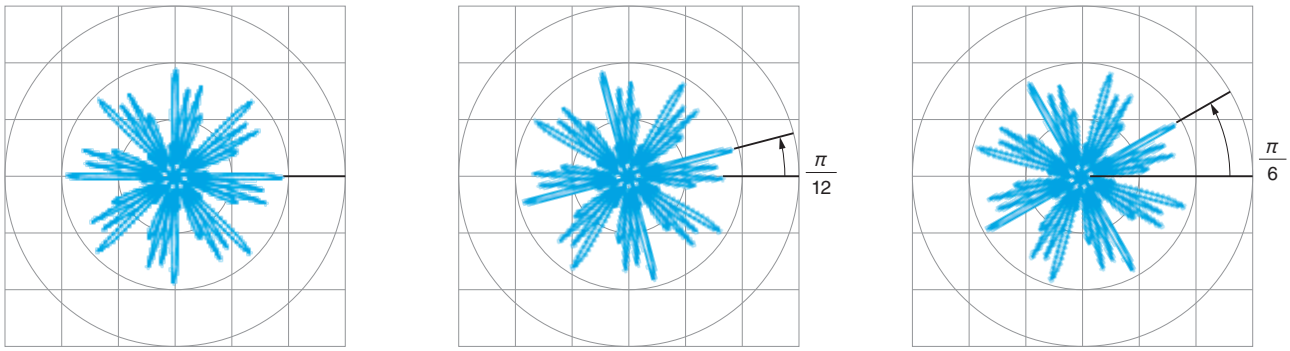

(a) t/Te = 0 (b) t/Te = 1/6 (c) t/Te = 1/3

Fig. 3 **Changes in Radial Electromagnetic Force with Time**

The diagrams show that the radial electromagnetic force is turning together with the rotor.

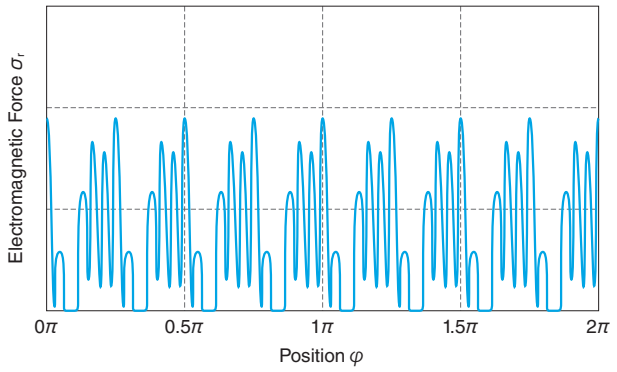

Fig. 4 **Spatial Distribution of Electromagnetic Force in Radial Direction**

The diagram indicates that the radial electromagnetic force involves periodicity.

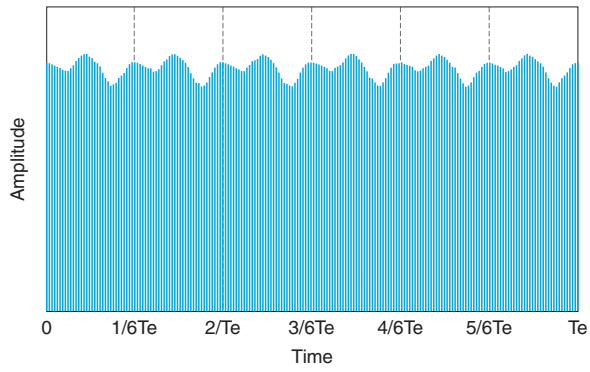

Fig. 6 **Change in Amplitude with Time for Nodal Diameter Number 8**

The diagram suggests that the radial electromagnetic force is turning together with the rotor, and is also changing in radial direction.

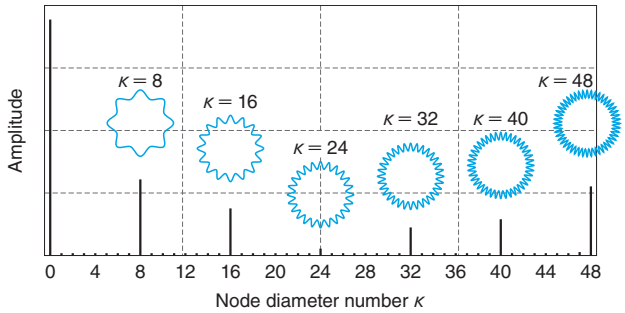

Fig. 5 **Relationship between Node Diameter Number and Amplitude**

The special distribution of radial electromagnetic force is superposed on the node diameter with integral multiples of 8.

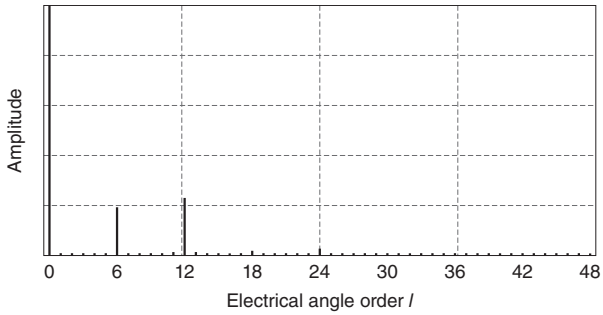

Fig. 7 **Relationship between Electrical Angle Order and Amplitude**

The electrical angle order tends to be high at 6th and 12th. This tendency suggests that there is radial variation at a frequency of 6fe and 12fe.

angle, it is indicated that the value increases at electrical angle order $l = 6$ and 12. In other words, there is variation in radial direction with a frequency at $l = 6$ and 12. As is recognized from **Fig. 6**, however, a change in amplitude with time at nodal diameter number $\kappa = 8$ brings out about 98% of DC component. Consequently, our research was carried on irrespective of changes in amplitude with time.

3 Clarification of Resonance Conditions

3.1 Equation of Motion and Expression of Diagonalization

Vibration analysis on periodic structures is frequently reported in regard to the turbine blades[2]. This thinking is applied to a 48-freedom system model of (b) shown in **Fig. 8** where the 48-slot stator core of (a) is assumed. In this case, it is assumed that 48 points of mass are distributed in peripheral direction, displacement of each mass in radial direction is defined as x_i $(i = 1 \sim 48)$, a spring between mass points is K_c, and a spring of each mass in radial direction is K_d. The phase between mass points is $\theta = 2\pi/48 = \pi/48$. On the assumption of displacement vector $\boldsymbol{X}_{48} = [x_1, x_2, \cdots x_{48}]^t$, the equation of motion for the 48-degree-of-freedom of the structural system is given by the following expression:

$$\boldsymbol{M}_{48}\ddot{\boldsymbol{X}}_{48} + \boldsymbol{K}_{48}\boldsymbol{X}_{48} = \boldsymbol{\sigma}_{48} f \cdots\cdots\cdots\cdots\cdots\cdots (2)$$

where, $\boldsymbol{M}_{48}$ is a mass matrix (48×48), $\boldsymbol{K}_{48}$ is a stiffness matrix (48×48), and $\boldsymbol{\sigma}_{48}$ an input matrix (48×1). Value f denotes a function of time for excitation. In the case of harmonic excitation for excitation frequency v, f is defined as $\cos vt$. The $\boldsymbol{M}_{48}$ matrix is a diagonal matrix where the respective mass points m are diagonally aligned.

$$\boldsymbol{M}_{48} = diagonal\,[m, m, \cdots, m]^t \cdots\cdots\cdots\cdots\cdots (3)$$

Since the $\boldsymbol{K}_{48}$ matrix is a periodic structure, it is given by the following expression:

$$\boldsymbol{K}_{48}\boldsymbol{X}_{48} = \begin{bmatrix} k_d+2k_c & -k_c & 0 & \cdots & 0 & 0 & -k_c \\ -k_c & k_d+2k_c & -k_c & \cdots & 0 & 0 & 0 \\ 0 & -k_c & k_d+2k_c & \cdots & 0 & 0 & 0 \\ \vdots & \vdots & \vdots & \ddots & \vdots & \vdots & \vdots \\ 0 & 0 & 0 & \cdots & k_d+2k_c & -k_c & 0 \\ 0 & 0 & 0 & \cdots & -k_c & k_d+2k_c & -k_c \\ -k_c & 0 & 0 & \cdots & 0 & -k_c & k_d+2k_c \end{bmatrix} \begin{bmatrix} x_1 \\ x_2 \\ x_3 \\ \vdots \\ x_{46} \\ x_{47} \\ x_{48} \end{bmatrix} \cdots\cdots (4)$$

To obtain a diagonal expression for Expression (2), coordinates transformation $\boldsymbol{W}$ is defined that is peculiar to the periodic structural system.

$$\boldsymbol{W} = \begin{bmatrix} e^{j\theta} & e^{2j\theta} & \cdots & e^{46j\theta} & e^{47j\theta} & 1 \\ e^{j2\theta} & e^{2j2\theta} & \cdots & e^{46j2\theta} & e^{47j2\theta} & 1 \\ \vdots & \vdots & \ddots & \vdots & \vdots & \vdots \\ e^{j46\theta} & e^{2j46\theta} & \cdots & e^{46j46\theta} & e^{47j46\theta} & 1 \\ e^{j47\theta} & e^{2j47\theta} & \cdots & e^{46j47\theta} & e^{47j47\theta} & 1 \\ 1 & 1 & \cdots & 1 & 1 & 1 \end{bmatrix}$$

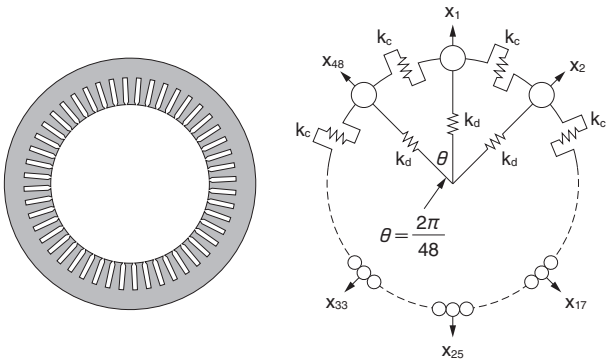

(a) Stator core shape (b) 48-freedom system model

Fig. 8 Stator Core Model

A stator core shape and a 48-freedom system model are shown.

$$= \begin{bmatrix} e^{j\theta} & e^{2j\theta} & \cdots & e^{-2j\theta} & e^{-j\theta} & 1 \\ e^{2j\theta} & e^{4j\theta} & \cdots & e^{-4j\theta} & e^{-2j\theta} & 1 \\ \vdots & \vdots & \ddots & \vdots & \vdots & \vdots \\ e^{46j\theta} & e^{92j\theta} & \cdots & e^{-92j\theta} & e^{-46j\theta} & 1 \\ e^{47j\theta} & e^{94j\theta} & \cdots & e^{-94j\theta} & e^{-47j\theta} & 1 \\ 1 & 1 & \cdots & 1 & 1 & 1 \end{bmatrix} \cdots\cdots (5)$$

In this expression, j comes in an imaginary unit and $\theta = 2\pi/48 = \pi/24$. This matrix is a symmetric matrix; $\boldsymbol{W} = \boldsymbol{W}^t$. When viewing the first to 47th columns, the first and 47th columns, second and 46th columns, $\cdots$, and 23th and 25th columns are in the relationship of conjugation. Namely, When the Kth column vector of $\boldsymbol{W}$ is expressed in $\boldsymbol{w}^t(K)$, the following expression is obtainable:

$$\boldsymbol{w}^t(K) = \overline{\boldsymbol{w}}^t(48 - K) \cdots\cdots\cdots\cdots\cdots\cdots\cdots (6)$$

Coordinates transformation using $\boldsymbol{W}$ above is then carried out.

$$\boldsymbol{X}_{48} \equiv \boldsymbol{W}\boldsymbol{Y}_{48} \equiv \boldsymbol{W}[y_1, y_2, y_3 \cdots, y_{48}]^t \cdots\cdots\cdots\cdots (7)$$

Practically, Expression (7) is substituted for Expression (2) and the transposed matrix of $\boldsymbol{W}$ is conjugated from the left. The result is a diagonal matrix as shown below.

$$\begin{aligned} \overline{\boldsymbol{W}}^t\boldsymbol{M}_{48}\boldsymbol{W} &\equiv \boldsymbol{M}^*_{48} = diagonal\,[m_1, m_2, m_3, \cdots, m_{48}] \\ &= m_t\,\boldsymbol{E}_{48} \cdots\cdots\cdots\cdots\cdots\cdots\cdots\cdots (8) \end{aligned}$$

In this case, however, $\boldsymbol{E}_{48}$ is an identity matrix of 48th dimension and m_t is a total mass $(48m)$.

$$\begin{aligned} \overline{\boldsymbol{W}}^t\boldsymbol{K}_{48}\boldsymbol{W} &\equiv \boldsymbol{K}^*_{48} = diagonal\,[k_1, k_2, k_3, \cdots, k_{24}, \cdots, k_{48}] \\ &= diagonal\,[k_1, k_2, k_3, \cdots, k_{23}, k_{24}, k_{23}, \cdots, k_1, k_{48}] \\ &\cdots\cdots (9) \end{aligned}$$

As a result, Expression (2) comes in 48 equations independent of each mode.

$$\begin{cases} m_t\ddot{y}_1 + k_1 y_1 = \overline{\boldsymbol{w}}^t(1)\boldsymbol{\sigma f} \\ m_t\ddot{y}_2 + k_2 y_2 = \overline{\boldsymbol{w}}^t(2)\boldsymbol{\sigma f} \\ m_t\ddot{y}_3 + k_3 y_3 = \overline{\boldsymbol{w}}^t(3)\boldsymbol{\sigma f} \\ \quad\vdots \\ m_t\ddot{y}_{23} + k_{23} y_{23} = \overline{\boldsymbol{w}}^t(23)\boldsymbol{\sigma f} \\ m_t\ddot{y}_{24} + k_{24} y_{24} = \overline{\boldsymbol{w}}^t(24)\boldsymbol{\sigma f} \\ m_t\ddot{y}_{25} + k_{23} y_{25} = \boldsymbol{w}^t(23)\boldsymbol{\sigma f} \\ \quad\vdots \\ m_t\ddot{y}_{47} + k_1 y_{47} = \boldsymbol{w}^t(1)\boldsymbol{\sigma f} \\ m_t\ddot{y}_{48} + k_{48} y_{48} = \overline{\boldsymbol{w}}^t(48)\boldsymbol{\sigma f} \end{cases} \cdots\cdots (10)$$

When a response of 1-degree-of-freedom per mode is taken into consideration, an idea of modal analysis is established where the total sum is a response from all. Because of separation per mode, natural frequency ω_K is given by Expression (11).

$$\omega_K^2 = \omega_{48-K}^2 = \frac{k_K}{m_t} \cdots\cdots (11)$$

3.2 Mode of the Coordinates Transformation Matrix *W*

Column K vector $\boldsymbol{w}^t(K)$ of transformation matrix $\boldsymbol{W}$ was examined below. The teeth number N for a round of the stator core is from 1 to 48. The Kth column $\boldsymbol{w}^t(K)$ of Matrix $\boldsymbol{W}$ is $\boldsymbol{w}^t(K) = [e^{Kj\theta}, e^{2Kj\theta}, \cdots, e^{47Kj\theta}, 1]^t$ for Number K up to 24. Regarding the displacement of the Nth tooth, the real part is cos $KN\theta = \cos\frac{\pi}{24}KN$ and the imaginary part is sin $KN\theta = \sin\frac{\pi}{24}KN$. The mode in this case is for nodal diameter $k = K$. The 24th column $\boldsymbol{w}^t(24)$ is a mode where the neighboring mass points move in antiphase action and the figure of nodal diameter is the largest. At the 25th column and thereafter, this action was turned back and the mode of the Kth column became nodal diameter $k = 48 - K$. At $K = 48$th column, $\boldsymbol{w}^t(48) = [1, 1, \cdots\cdots, 1]^t$. This is an in-phase mode when all mass points make the same actions. Fig. 9 shows the modal shape of Matrix $\boldsymbol{W}$. K is a column of Matrix $\boldsymbol{W}$ and k is the nodal diameter of this mode. The upper stage (a) shows a mode that was established by the real part of the column vector and the lower stage (b) shows a mode established by the imaginary part.

3.3 Modal Exciting Force and Resonance Conditions

For the electromagnetic excitation force σ distributed in the peripheral direction of the stator core, one round is put into Fourier transformation to obtain Expression (12) below.

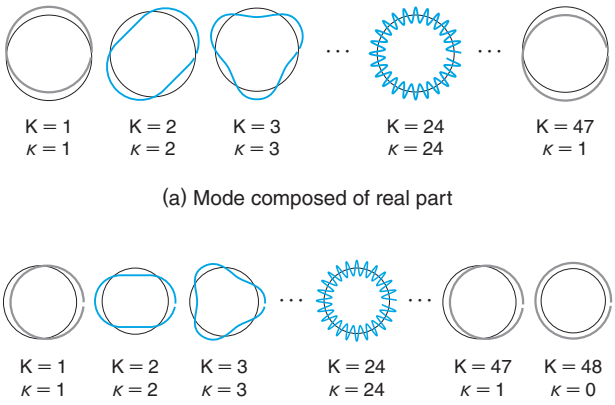

(a) Mode composed of real part

(b) Mode composed of imaginary part

Fig. 9 Modal Shape of Matrix W

Modal shapes of Matrix W and column vector are shown.

$$\sigma(\varphi) = b_0 + \sum_{J=1}^{\max}\{b_{cJ}\cos(j\varphi) + b_{sJ}\sin(j\varphi)\} \cdots (12)$$

where, $\varphi = 0 \sim 2\pi$, b_0 is a DC component, b_{cf} is an amplitude of cosine component of the Jth harmonic, and b_{sf} is an amplitude of sine component of the Jth harmonic. Consequently, the modal excitation force is $\overline{\boldsymbol{W}}^t\boldsymbol{\sigma}$ and it is the right side of Expression (10). This value is existent when the Kth mode coincides with the order number J of the excitation mode, i.e. $K = J$.

For example, let's consider the case of $K = J = 1$. The mode at $K = 1$ is given by Expression (13) below.

$$\begin{aligned} \overline{\boldsymbol{w}}(1) &= [e^{-j\theta}, e^{-2j\theta}, \cdots, e^{-47j\theta}, 1] \\ &= [\cos\varphi - j\sin\varphi] \cdots\cdots (13) \end{aligned}$$

In this case, $\varphi = n\theta$ and $n = 1 \sim 48$. When $\overline{\boldsymbol{w}}(1)$ is multiplied by Component $\sigma(\varphi)$ of excitation force in Expression (12) and is then integrated, only the expression of $\sigma(\varphi) = b_{c1}\cos\varphi + b_{s1}\sin\varphi$ remains at $J = 1$. The participation factor $\overline{\boldsymbol{W}}^t\boldsymbol{\sigma}$ is given by Expression (14) below.

$$\begin{aligned} \overline{w}\sigma(\varphi) &= \int_0^{2\pi}(\cos\varphi - j\sin\varphi)(b_{c1}\cos\varphi + b_{s1}\sin\varphi)\,d\varphi \\ &= \pi(b_{c1} - jb_{s1}) \cdots\cdots (14) \end{aligned}$$

When Expression (10) is rewritten, and is attached with modal damping ratio ζ_i to express an equation of motion for each mode, Expression (15) is obtainable.

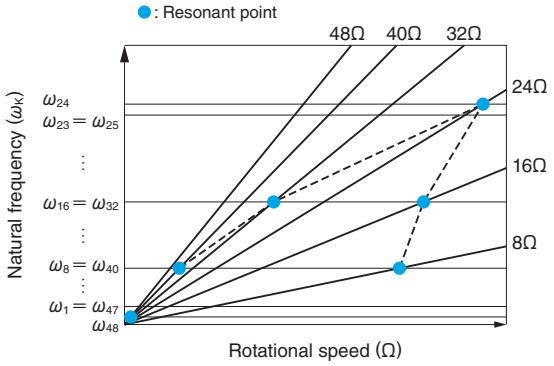

Fig. 10 **Campbell Diagram**

The diagram indicates that resonance is caused at Mark ● where the condition for resonance is satisfied.

$$\begin{cases} m_t(\ddot{y}_1 + 2\zeta_1\,\omega_1\,\dot{y}_1 + \omega_1^2 y_1) = \pi(b_{c1} - jb_{s1})f \\ m_t(\ddot{y}_2 + 2\zeta_2\,\omega_2\,\dot{y}_2 + \omega_2^2 y_2) = \pi(b_{c2} - jb_{s2})f \\ m_t(\ddot{y}_3 + 2\zeta_3\,\omega_3\,\dot{y}_3 + \omega_3^2 y_3) = \pi(b_c 3 - jb_{s3})f \\ \quad\vdots \\ m_t(\ddot{y}_{24} + 2\zeta_{24}\,\omega_{24}\,\dot{y}_{24} + \omega_{24}^2 y_{24}) = \pi(b_{c24} - jb_{s24})f \\ m_t(\ddot{y}_{25} + 2\zeta_{23}\,\omega_{23}\,\dot{y}_{25} + \omega_{23}^2 y_{25}) = \pi(b_{c23} + jb_{s23})f \\ \quad\vdots \\ m_t(\ddot{y}_{47} + 2\zeta_1\,\omega_1\,\dot{y}_{47} + \omega_1^2 y_{47}) = \pi(b_{c1} + jb_{s1})f \\ m_t(\ddot{y}_{48} + 2\zeta_{48}\,\omega_{48}\,\dot{y}_{48} + \omega_{48}^2 y_{47}) = 2\pi b_0 f \end{cases} \quad \cdots\cdots (15)$$

When Expression (15) is summed up, the resonance conditions are available in the following two cases.

(1) $K = J$, where the inner product of mode shape $\overline{\boldsymbol{W}}^t$ and electromagnetic excitation force $\boldsymbol{\sigma}$ is existent.

(2) $v = \omega_K$, where excitation frequency v coincides with natural frequency ω_K.

Fig. 10 shows the Campbell diagram. The axis of ordinates shows the natural frequency of the stator core and that of abscissas shows the rotational speed of the rotor. The oblique lines show the excitation frequency when the Jth electromagnetic excitation force is applied at the rotational speed f_r. By the effect of electromagnetic force in **Section 2**, the distribution of electromagnetic force in radial direction working as an excitation force results in the order number in peripheral direction that is a multiple of 8, i.e. $J = 8$, 16, 24, 32, 40, and 48. When the values meeting the resonance conditions of (1) and (2) above are added to the Campbell diagram, it can be recognized that resonance can be caused at Mark ● in **Fig. 10**.

4 Postscript

This paper introduced the resonance conditions caused in the IPMSM. It is possible to predict the resonance point by making detailed electromagnetic field analysis and adequate modeling approach. When the result of this study is applied, it is possible to realize a resonance averting design for the stator core. This achievement will contribute to the improvement of acoustic vibration characteristics for the IPMSM.

Lastly, we would like to express our sincere gratitude to Professor Emeritus Matsushita of The National Defense Academy for his precious advices, guidance, and theoretical examinations during our R&D activities in regard to sound vibration analytical technologies.

(Note)

※1. Fourier transformation: A process where functions with variables of time and special coordinates are converted into those with variables of frequency.

《References》

(1) Yoshinari Asano, Yukio Honda, Yoji Takeda, Shigeo Morimoto: "Reduction of Vibration Focused on Radial Stresses of Concentrated Winding Permanent Magnet Synchronous Motor," Theses of the Institute of Electrical Engineers of Japan D, Vol.121, No.11, pp.1185～1191, 2001 (in Japanese)

(2) Osami Matsushita, Masato Tanaka, Hiroshi Kamiyoshi, Masao Kobayashi: "Basics of Practical Vibration Analysis for Vibration in Rotary Machines," Corona Inc., pp.227～258 (in Japanese)